Elabd and Hussein *J Wireless Com Network* (2023) 2023:109
https://doi.org/10.1186/s13638-023-02321-9

EURASIP Journal on Wireless Communications and Networking

RESEARCH **Open Access**

Efficient design of a wideband tunable microstrip filtenna for spectrum sensing in cognitive radio systems

Rania H. Elabd[1*] and Amr H. Hussein[2,3]

*Correspondence: Eng.rania87@yahoo.com; rania.hamdy@ndeti.edu.eg

[1] Electronics and Communications Engineering Department, High Institute of Engineering and Technology, New Damietta, Egypt
[2] Electronics and Electrical Communications Engineering Department, Faculty of Engineering, Tanta University, Tanta, Egypt
[3] Electronics and Electrical Communications Engineering Department, Faculty of Engineering, Horus University Egypt, New Damietta, Egypt

Abstract

This paper presents a novel design of a compact, wideband tunable microstrip filtenna system for effective spectrum sensing in cognitive radio (CR) applications. The proposed filtenna structure has a total bandwidth of 1.63 GHz and flexible frequency scanning design throughout the frequency range from 1.93 to 3.56 GHz with high selectivity and narrow bandwidths ranging from 39.9 to53 MHz. Frequency tuning is accomplished electrically via integrating a varactor diode into the filtenna construction. The filtenna is realized on a Rogers TMM4 substrate with $h = 1.52$ mm thickness and relative dielectric constant of $\varepsilon_r = 4.5$ with dimensions of (25×35) mm^2. The obtained gain and efficiency of the filtenna ranged from 0.7 to 2.26 dBi and 49% to 60%, respectively, within the tuning range. Simple biasing circuitry, wideband operation, and compact planar structure are distinctive and appealing aspects of the design. For the manufactured prototypes, a significant level of agreement is found between the simulated and measured results in terms of scattering parameter S_{11} and radiation patterns at different operating frequencies.

Keywords: Cognitive radio (CR), Filtenna, Microstrip antenna, Spectrum sensing (SS), Tunable filtenna

1 Introduction

As a result of the tremendous development of wireless applications, several frequency bands are crowded. In contrast, others are scarcely used, and more challenges have emerged as the electromagnetic environments get increasingly complicated [1]. Consequently, one of the potential answers for upcoming wireless communications is the cognitive radio (CR) concept [2, 3]. CR can effectively address the issues of next-generation spectrum utilization. Spectrum sensing is a fundamental step for efficient CR, whereby unlicensed or secondary users (SU) must constantly check the spectrum for the presence of authorized/primary users (PUs). The implementation of spectrum sensing to detect the least amount of inactive spectrum affects a CR system's spectral efficiency [4].

There are several methods for boosting capacity, including CR [1–4], multiple-input multiple-output (MIMO) [5–9], and discrete wavelet transforms (DWT). To increase spectral efficiency, DWTs are used in orthogonal frequency division multiplexing

(OFDM) systems. In order to increase system performance and spectrum efficiency, antenna diversity schemes may be designed using wavelet transforms [10–14] as well as the efficient design of the antenna element used in the antenna array system. The recent advances in software-defined radio (SDR) and dynamic spectrum allocation have created new difficulties in reconfigurable antenna design. Because of their ability to adjust their operating frequency and maintain the same radiation and gain characteristics, reconfigurable antennas are gaining popularity. Maintaining a consistent gain in multiple resonant modes of the structure is one of the most challenging issues in reconfigurable antenna design for practical applications. Integrating a reconfigurable filter with the antenna construction is a promising solution. Because this technique will not change the antenna surface current distribution, the frequency tuning of the filter will have a negligible impact on the antenna radiation pattern [15]. This will increase the flexibility of frequency of the sensing element that enables the CR system to learn and change to the RF environment.

Since antennas and filters are often the biggest components in wireless communication systems, there is interest in developing a single module that merges these components while keeping the filtering and radiation properties of each element. Filtenna, which combines a tunable filter and antenna, has recently been developed [15]. As opposed to joining distinct filter and antenna components, adding an antenna element to a tunable filter produces a consistent gain and fixed radiation pattern. The filtenna integration technique simplifies the impedance matching between the antennas and filter components, controls the return losses, and minimizes the system size, which are attractive features of filtenna systems [16–18]. For cognitive radio applications, reconfigurable filtenna that can be adjusted mechanically, electrically, and optically were introduced in [19–30]. Electrical frequency reconfiguration is the most commonly used technique that can be accomplished either by utilizing a PIN diode [29–31] or a varactor diode [22–30]. Although the filtenna module introduced in [18] was formed by the direct connection of independent antenna and filter to achieve the desired characteristics, the module did not produce predictable results since the filter response deteriorated owing to module impedance mismatch brought on by the two elements connection. Size reduction is another benefit of the antenna-filter integration strategy, which minimizes impedance mismatch losses [19]. However, regarding selectivity parameters and band-rejection properties, the systems did not generally exhibit acceptable performance. On the other hand, the ability to integrate filters directly into antenna feed lines made it feasible to reduce the size of the communication system's front end, and the inherent flexibility of these systems assured adaptability.

In [20], the authors produced reconfigurability using two PIN diodes. The design achieved 0.9 GHz tuning band from 3.3 to 4.2 GHz, gain of 3.5 dBi, and 50% efficiency. In [21], the authors also designed reconfigurability using two PIN diodes with 1.07 GHz tuning band from 3.63 to 4.7 GHz, and gain of 2 dBi.

In [22], the authors presented reconfigurability using four varactor diode. The design achieved 1.25 GHz tuning band from 1.75 to 3GHz, and gain of 4.5 dBi, but it suffers from large design size. In [23], the authors designed a band-pass filter (BPF) integrated with a wideband (WB) monopole antenna. This was done by using two coupled defected ground structure (DGS) resonators and two coupled microstrip lines ended with two stubs. They displayed tunability using four varactor diodes. Their design achieved 1.7 GHz tuning band from 1.3 to 3 GHz. In [23, 25], the authors highlighted reconfigurable antenna design that has high gain with small tuning range. In [12, 14], and [25], authors utilized single varactor diodes to achieve reconfigurability, but their designs suffer from low gain and large size.

In [26], the filtenna tunability has been achieved by a variable capacitor placed in the middle of the largest side of the trapezoid truncated in the ground plane.

A lot of research investigated various designs of the filtenna for size reduction of the RF front end as in [27–32].

In [33] and [34], a band-pass filter was incorporated into the feed line of an ultra-wideband (UWB) patch antenna. The reconfiguration was done using selected keys modeled as copper tapes, producing the two system operation modes: broadband and narrowband modes. Because it was essential to short-circuit some elements of the structure in order to transition between the modes of operation, reconfiguration proved a challenging issue to carry out.

A similar strategy is applied in [35]; however, this time the reconfiguration is carried out using PIN diodes. The design provided a broadband operation via the ON and OFF diode states, allowing for the rejection of frequencies of 5.25 GHz or 5.8 GHz in accordance with PIN diode bias. A 30 dB attenuation was achieved with this combination, which had good results.

The utilization of multiple antenna elements or antenna arrays gained significant attention in the field of spectrum sensing. In [36] and [37], two antenna array beam forming techniques were introduced for performance enhancement of spectrum sensing process. In [36], maximum gain realization of the antenna array was discussed, while in [37], side lobe-level reduction was investigated. Both techniques significantly improved the spectrum sensing process in cognitive radio systems.

In this paper, a compact microstrip filtenna with dimensions of $(25 \times 35)\,\mathrm{mm}^2$ to sense the frequency spectrum from 1.95 to 3.95 GHz is introduced. The frequency tuning is accomplished electrically by combining a varactor diode into the filtenna construction. The filtenna is implemented on a Rogers TMM4 substrate having a thickness $h = 1.52\,\mathrm{mm}$ and a relative dielectric constant $\varepsilon_r = 4.5$. This area of the spectrum was picked as it contains the 2.45 GHz Industrial Scientific Medical (ISM) frequency band, which is congested. Wi-Fi, Bluetooth, and ZigBee networks plus numerous additional appliances operate in this spectrum, which is typically unlicensed.

The main contributions of this paper are listed below:

I. A compact wideband filtenna was proposed, and it achieved a bandwidth of 2.7 GHZ from 1.3 GHz to more than 4 GHz, with high efficiency and gain of 98.7% and 5.7 dB, respectively.
II. The proposed reconfigurable BPF has a compact size with a total physical dimension of $(20 \times 20)\,\mathrm{mm}^2$, a resonance frequency of 2.2 GHz, high selectivity with a fractional bandwidth of 8%, a return loss of 22 dB, and an insertion loss of 1 dB.
III. The reconfigurable BPF is developed using a single varactor diode with tuning frequency range from 1.95 to 3.95 GHz, while some other BPFs are developed using 4 varactor diodes, which complicates the filter design and tuning process.

IV. The proposed filtenna was obtained by integrating the WB antenna and the reconfigurable BPF, where the tunable BPF is inserted into the feed line of the WB antenna. It achieved a wide tuning frequency band of 1.63 GHz, which spans the range from 1.93 to 3.56 GHz.
V. The realized gain and efficiency of the filtenna ranged from 0.7 to 2.26 dBi and 49% to 60%, respectively, within the tuning range.

The remainder of the paper is structured as follows: The method and experiment of the suggested filtenna structure's design steps are detailed in Sect. 2. The suggested filtenna result and discussion are presented in Sect. 3. The comparison between the suggested filtenna and state-of-the-art works is presented in Sect. 4. The paper is concluded in Sect. 5.

2 Method and experiment

In this section, a new design for an efficient frequency-tunable filtenna is introduced for cognitive radio application. The proposed filtenna is designed and simulated on a Rogers TMM4 substrate having a thickness of $h = 1.52$ mm and a relative dielectric constant $\varepsilon_r = 4.5$. The simulations are carried out using the computer simulation technology (CST) microwave studio software package (CST-MWS-2019). The suggested frequency-tunable filtenna design procedure is divided into four main stages: (A) antenna element design for wide band (WB) with moderately flat gain characteristic, (B) plan of the suggested square open lope resonator (SOLR)-based BPF, (C) incorporating the varactor diode to the designed BPF to make it tunable with high selectivity, and (D) incorporating the WB antenna and the tunable BPF in a single scheme to create filtenna as shown in Fig. 1.

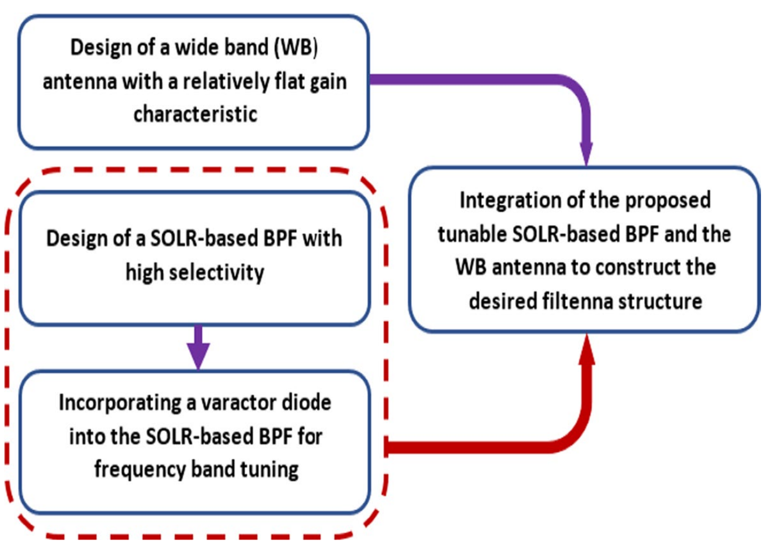

Fig. 1 Flowchart of the design procedure of the suggested filtenna

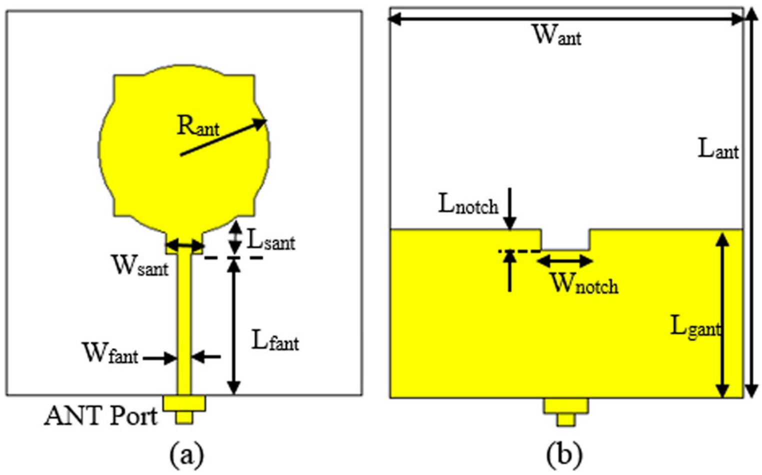

Fig. 2 The geometrical structure of the proposed circular-shaped wideband antenna element; **a** Top view, **b** Bottom view

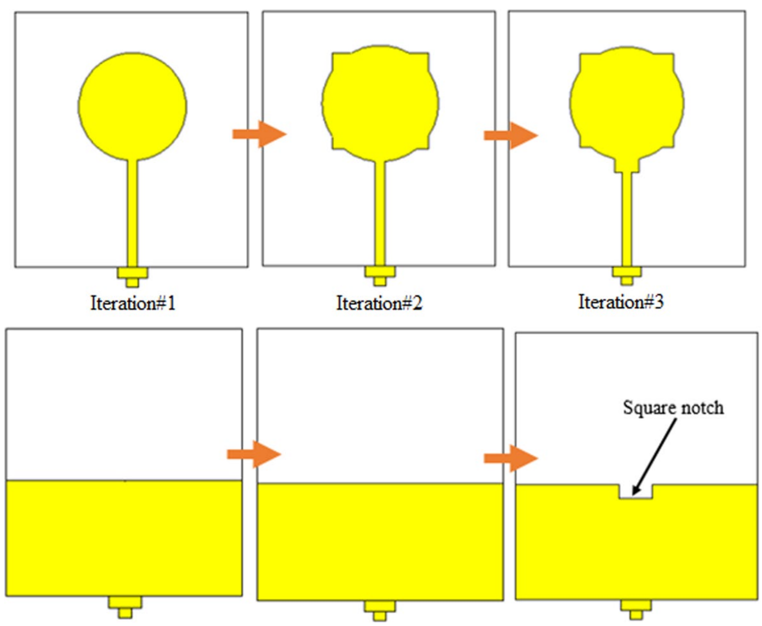

Fig. 3 Progressive design iterations of the circular-shaped wideband antenna element

2.1 Design of the proposed wideband antenna element

In this section, the CST design procedures, prototype fabrication, and experimental measurements of a new design for a WB circular-shaped antenna element are introduced. The proposed antenna structure is composed of a circular radiating patch with four semi-squared stubs and square notch-loaded ground plane. The final geometrical structure of the designed antenna element is illustrated in Fig. 2.

The design steps of the proposed WB circular-shaped antenna are shown in Fig. 3. Iteration#1 shows the design of a conventional circular radiating patch with a partial ground plane. The initial value of the circular patch radius is calculated by [38]:

$$R = \frac{G}{\left\{1 + \frac{2h}{\pi \varepsilon_r G}\left[ln\left(\frac{\pi G}{2h}\right) + 1.7726\right]\right\}^{1/2}} \quad (1)$$

$$G = \frac{8.791 \times 10^9}{f_r \varepsilon_r} \quad (2)$$

where $R =$ The radius of the circular radiating patch in cm. $h =$ The thickness of the substrate in cm. $\varepsilon_r =$ The relative dielectric constant of the substrate $f_r =$ The required resonance frequency.

While the optimal value of the circular patch radius is determined by using the CST simulator optimization, such structure provides a wide operating frequency band from 1.3 to 4 GHz but with high return losses around the 3 GHz frequency, as shown in Fig. 4. That is due to the sudden variance in the impedance at the point of junction of the radiating patch and the feed line.

In iteration#2, four tiny fractal squares (1.2×1.2) mm^2 are added to the circular patch to improve the return loss of the antenna. This results in the same operating frequency band from 1.3 to 4 GHz but with moderate return loss around the 3 GHz frequency as shown in Fig. 4.

In iteration#3, a square slit is etched on the top side of the partial ground plane, and two square stubs are added under the circular radiating patch on both sides of the feeding line that increases the electrical length of the radiating patch and improves the bandwidth and achieving better impedance matching across the entire frequency range. This final structure improved the antenna return loss in the operating frequency band from 1.3 to 4GHz with scattering parameter $-48\,\text{dB} \leq |s_{11}| \leq -14\,\text{dB}$ as shown in Fig. 4. The optimal dimensions of the proposed antenna structure are given in Table 1. The antenna is printed on a Rogers TMM4 substrate having a thickness $h = 1.52$ mm and a relative dielectric constant $\varepsilon_r = 4.5$ with a total area of (25×35) mm^2. By considering the final antenna design structure derived from iteration #3, the realized antenna gain versus frequency is shown in Fig. 5. The antenna provides a considerable gain ranging from 1.6to 4.7 dBi over the operating frequency band from 1.3to 4 GHz. Furthermore, it provides high radiation efficiency ranging from 89 to 98.8% over the operating frequency band

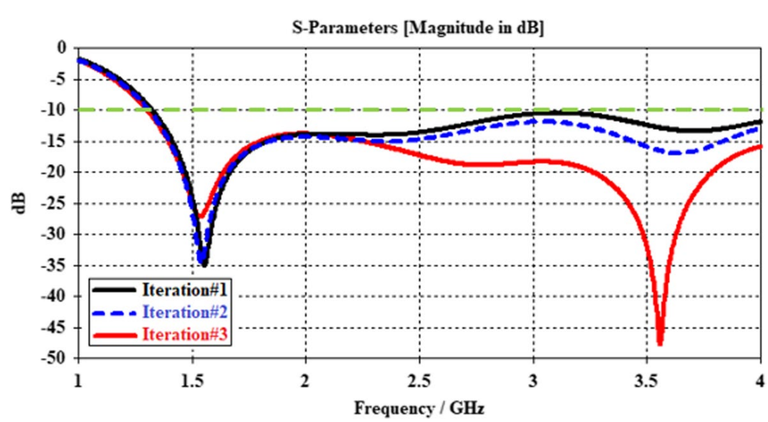

Fig. 4 The simulated reflection coefficient $|s_{11}|$ of the proposed wide band antenna procedures

Table 1 Dimensions of the proposed circular-shaped wideband antenna element in (mm)

Parameter	Value (mm)	Parameter	Value (mm)
W_{ant}	25	R_{ant}	7
L_{ant}	35	W_{sant}	2.5
W_{notch}	3	L_{sant}	2
L_{notch}	1	W_{fant}	2.04
L_{gant}	13.6	L_{fant}	14

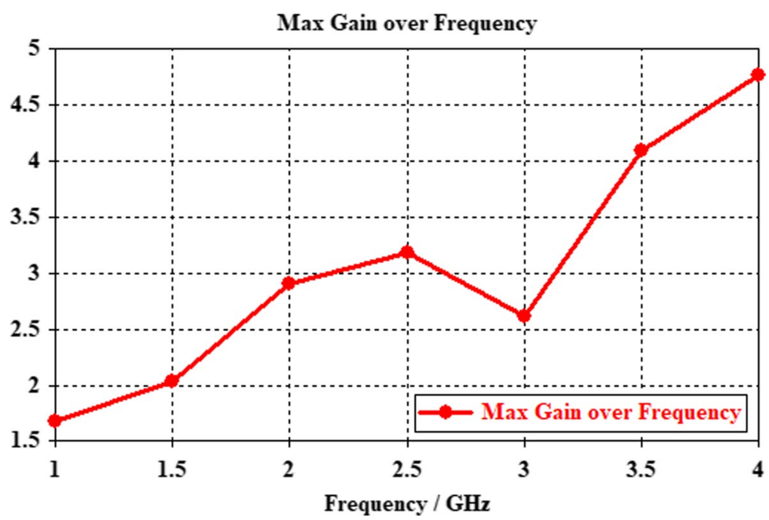

Fig. 5 The simulated gain of the proposed wide band antenna

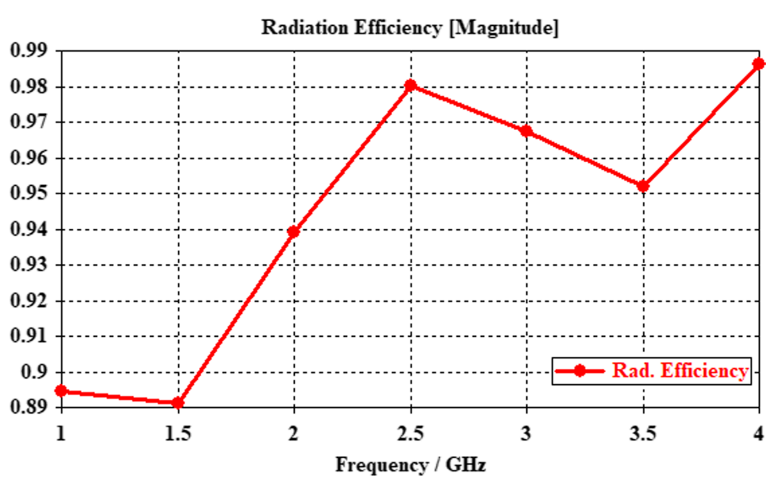

Fig. 6 The simulated radiation efficiency of the proposed wide band antenna

1.3to 4 GHz as shown in Fig. 6. Also, the real part of the antenna reference impedance is constant and equals 50Ω as shown in Fig. 7.

The fabricated prototype of the proposed wideband antenna is shown in Fig. 8. The scattering parameter $|s_{11}|$ of the proposed wideband antenna is measured using

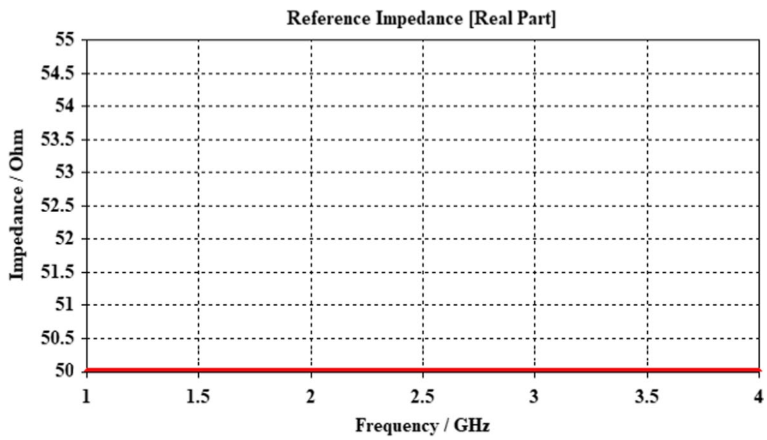

Fig. 7 The simulated real part of the antenna reference impedance for the proposed wide band antenna

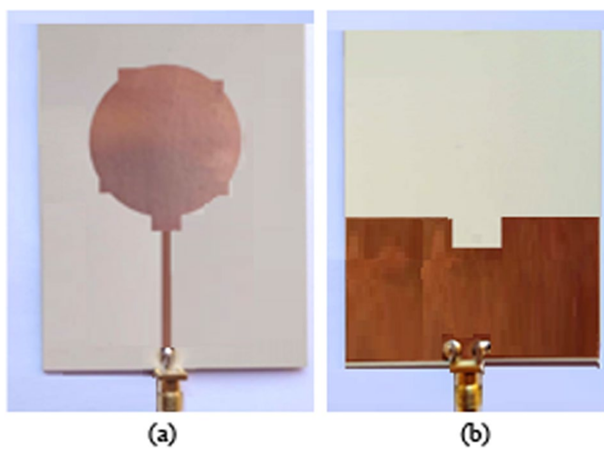

Fig. 8 Fabrication of the proposed wide band antenna **a** top view, **b** bottom view

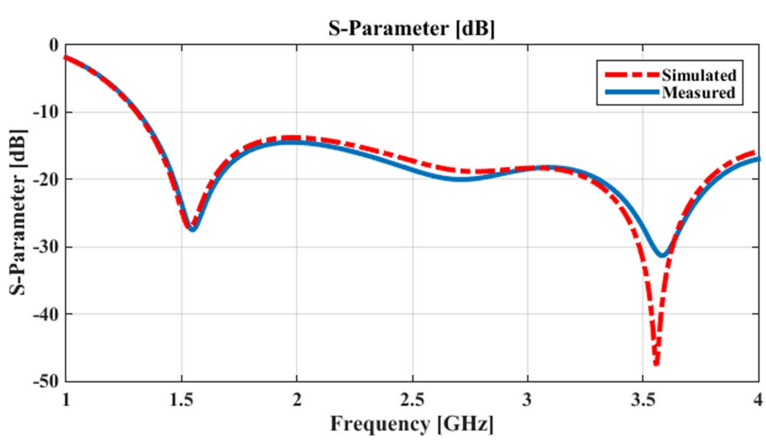

Fig. 9 The simulated and measured reflection coefficient $|s_{11}|$ of the proposed wide band antenna element

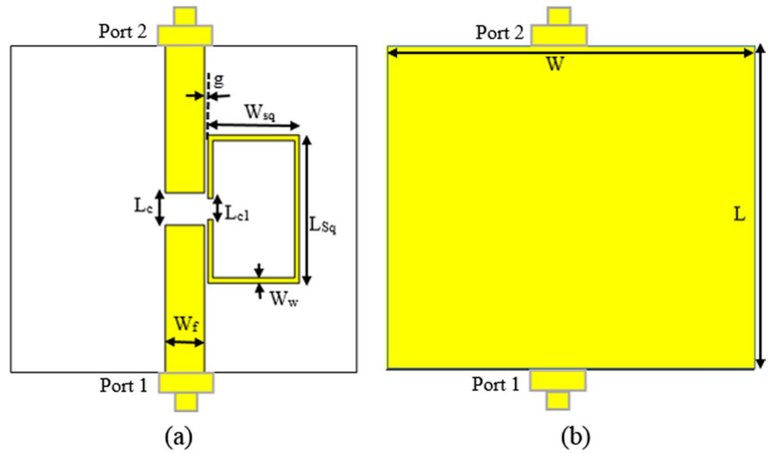

Fig. 10 Proposed SOLR-based BPF structure **a** Front view. **b** Back view

Table 2 Dimensions of the proposed SOLR-based BPF in (mm)

Parameter	**Value** (mm)	**Parameter**	**Value** (mm)
W	20	g	0.75
L	20	W_w	1
W_f	3.06	L_{sq}	12
L_c	2.5	L_{c1}	1.5
W_{sq}	6.7		

the Rohde & Schwarz ZVB 20 vector network analyzer as shown in Fig. 9. The $|s_{11}|$ is below the − 10 dB in the entire frequency range from 1.3 GHz to more than 4 GHz. A good agreement between the simulated and measured results is observed. But, due to fabrication tolerance values, there is little discrepancy between the simulation and measurement results.

2.2 Design of the proposed SOLR-based BPF

Herein, we outline our proposed BPF's design. The SOLR (square open lope resonator) structure is the principal founder of this design. The geometrical structure of the proposed BPF is illustrated in Fig. 10. Table 2 contains the suggested filter's dimensions in mm. Firstly, as described in Fig. 10, a fixed capacitance structure is made by etching a thin gap in width L_c in the middle of the stripe line. Figure 11a shows that the capacitances Cp and Cg are used to simulate the etched gap. The capacitance Cg results from the interaction between the coplanar lines, whereas the capacitance Cp is the capacitance caused by the interaction of the feed line with the ground plane. The values of both capacitances can be obtained using [39], and [40].

Controlling the connection between the two transmission line portions is necessary, and a SOLR is placed close to the stripe line. Figure 11b depicts the SOLR cell's equivalent circuit model. The SOLR behaves as an externally driven LC resonant circuit [41]. The length L_{sq} of the SOLR specifies the operating frequency of the filter.

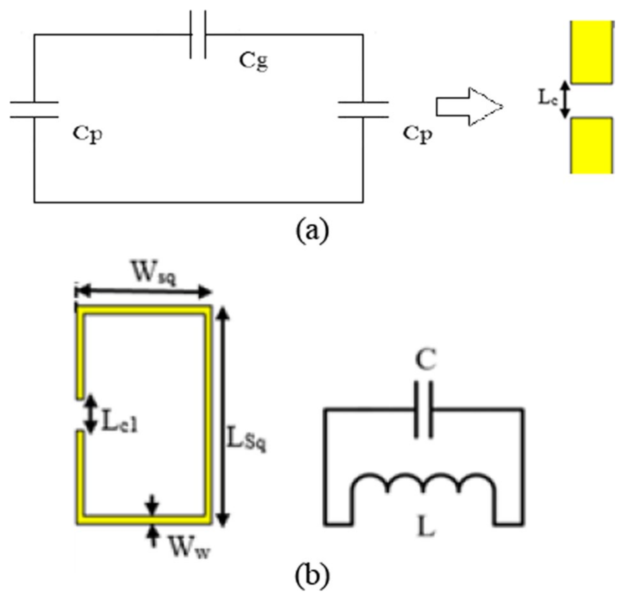

Fig. 11 **a** Equivalent circuit model for a gap between microstrip lines. **b** Equivalent circuit model of general structure of a SOLR cell

In order to gain a better understanding how the suggested BPF behaves, we convert the microstrip structure to its equivalent LC model.

The suggested topology is symmetric, making it simple to use half-circuit LC analysis to convert the microstrip transmission lines to the LC model, as illustrated in Fig. 12a considering lossless microstrip transmission lines. The inductances of the central transmission lines are represented in this LC model by the parameters L1 to L9. C1 is used to model the capacitance effect of the gap between the two feed lines. C2 and C3 represent the capacitance effect of the gap between the feed line and the resonator. C8 and C9 represent the capacitance effects of the open stubs with respect to the ground. The capacitance effects of the bends are also represented by the values C3 to C6.

Every component of the microstrip line is then converted to an equivalent LC component after being divided into smaller sections to assist the conversion process. Finally, the electrical values of each element are determined using the calculation method provided in [42].

A number of simulations were completed by fine-tuning the acquired values of each LC model component in order to establish a better fit between the simulation results of the EM and the converted circuit. The LC equivalent circuit of the proposed BPF was simulated using the electromagnetic simulator ADS. The proposed BPF's schematic circuit model is shown in Fig. 12b using the ADS simulation tool. The simulated scattering parameters of the LC model using ADS are shown in Fig. 12c. It is noticed that the behavior of the BPFs is ideal and allows them to pass frequency 2.191 GHz at values of the LC components as follows: $L_1 = 0.01$, $L_2 = 0.01$, $L_3 = 0.01$, $L_4 = 0.01$, $L_5 = 0.01$, $L_6 = 0.01$, $L_7 = 0.009$, $L_8 = 0.01$, $L_9 = 0.01$ (all in nH). $C_1 = 4.2$,$C_2 = 1\mathrm{e}-6$, $C_3 = 0.18$, $C_4 = 1\mathrm{e}-6$, $C_5 = 0.12$, $C_6 = 0.12$, $C_7 = 0.15$, $C_8 = 7.4$, $C_9 = 6$, $C_{10} = 0.12$(all in pF).

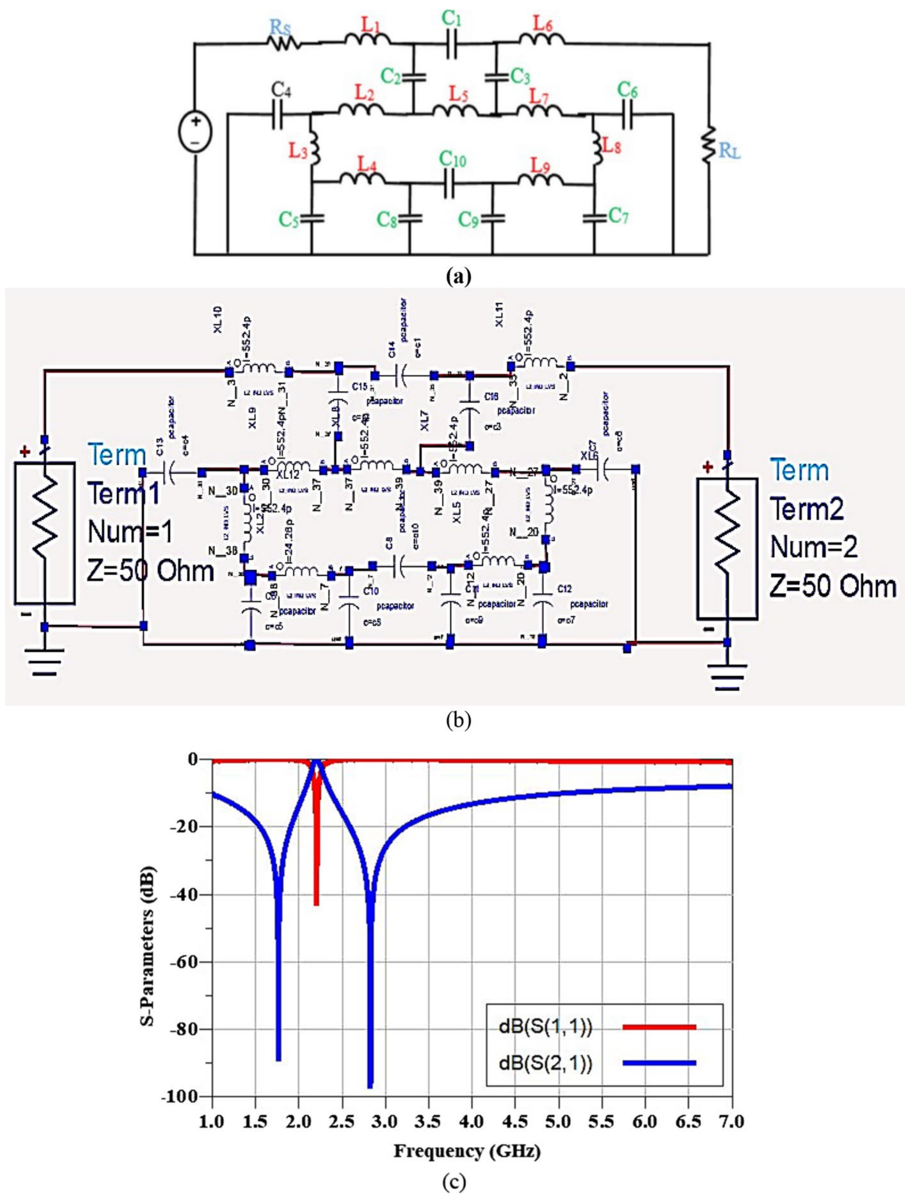

Fig. 12 **a** The proposed BPF's LC equivalent circuit. **b** The schematic circuit model of the proposed BPF in ADS simulation program. **c** Scattering parameter of proposed BPF equivalent circuit in ADS simulation program

The CST simulation results of the suggested SOLR-based BPF are displayed in Fig. 13. The BPF has a center frequency of 2.2 GHz, a fractional bandwidth of 8 %, a return loss of 22 dB, and an insertion loss of 1 *dB*.

2.3 Tunable SOLR-based BPF design

The suggested SOLR-based BPF introduced in section B is updated in this subsection to function as a tunable BPF. As shown in Fig. 14, the SMV1405 varactor diode from Skyworks Inc. is linked across the thin gap etched at length (L_{sq}) of the SOLR's center for dynamic frequency tuning. Figure 15 describes the varactor's equivalent circuit.

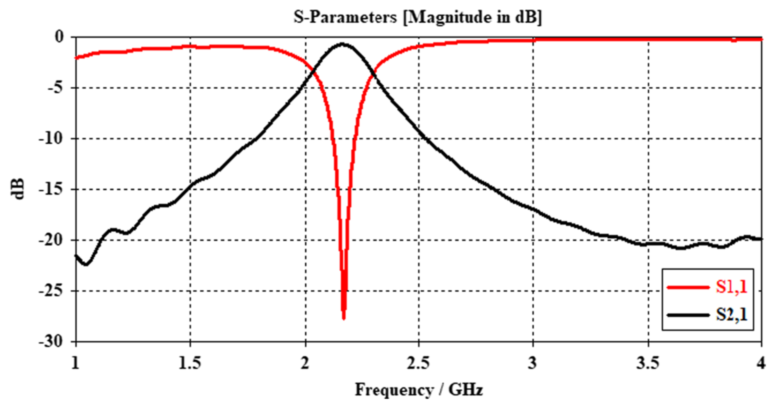

Fig. 13 Scattering parameter of proposed BPF in CST simulation program

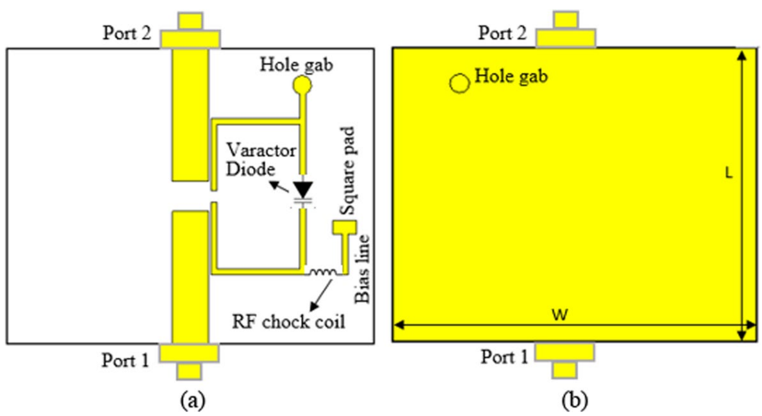

Fig. 14 Proposed tunable BPF construction **a** Front view. **b** Back view

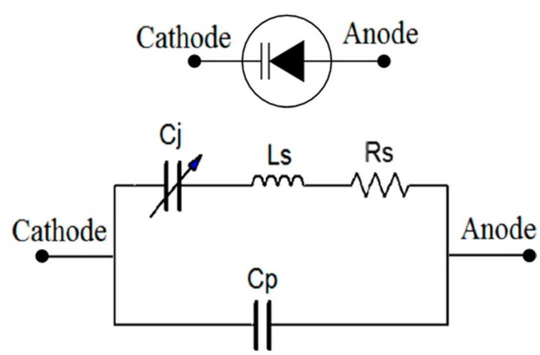

Fig. 15 The varactor diode's equivalent circuit where $LS = 0.7$ nH, $RS = 0.8\Omega$, and $Cp = 0.05$ pF

The cathode of the varactor is joined to the edge of the SOLR which is connected to the bias line through a choke coil which is linked to the DC supply over a square pad. The width and length of bias line have 0.75 mm 5 mm, respectively. It terminates with a square pad where the DC wire can be joined. The varactor's anode is linked to the edge of the SOLR, which is joined to the stub, which in turn is joined to the ground plane via a hole gap of 1mm diameter. In order to avoid RF leakage to the DC power supply, a choke coil is inserted between the stub and SOLR. This work uses a Murata LQM18N choke coil with a 47 nH inductance.

The junction capacitance *Cj* varies from 2.67 to 0.63 pF, by adjusting the varactor's DC voltage from 0 to 30 Volts. Therefore, the simulated operating frequency is changed from 1.95 to 3.95 GHz. The simulated scattering parameters $|s_{11}|$ and $|s_{12}|$ of the tunable BPF are drawn against frequency as shown in Fig. 16. It is evident that the simulated $|S_{11}|$ is less than −14dB over the tuning frequency range from 1.95 to 3.95 GHz. Table 3 lists the filter's simulated insertion losses (IL) at various resonance frequencies. As a result of the varactor diode circuit losses, it is relatively high. It is evident from Table 2's calculation of the filter's 10 dB bandwidth that the filter offers high selectivity with a constrained bandwidth of less than 60 MHz.

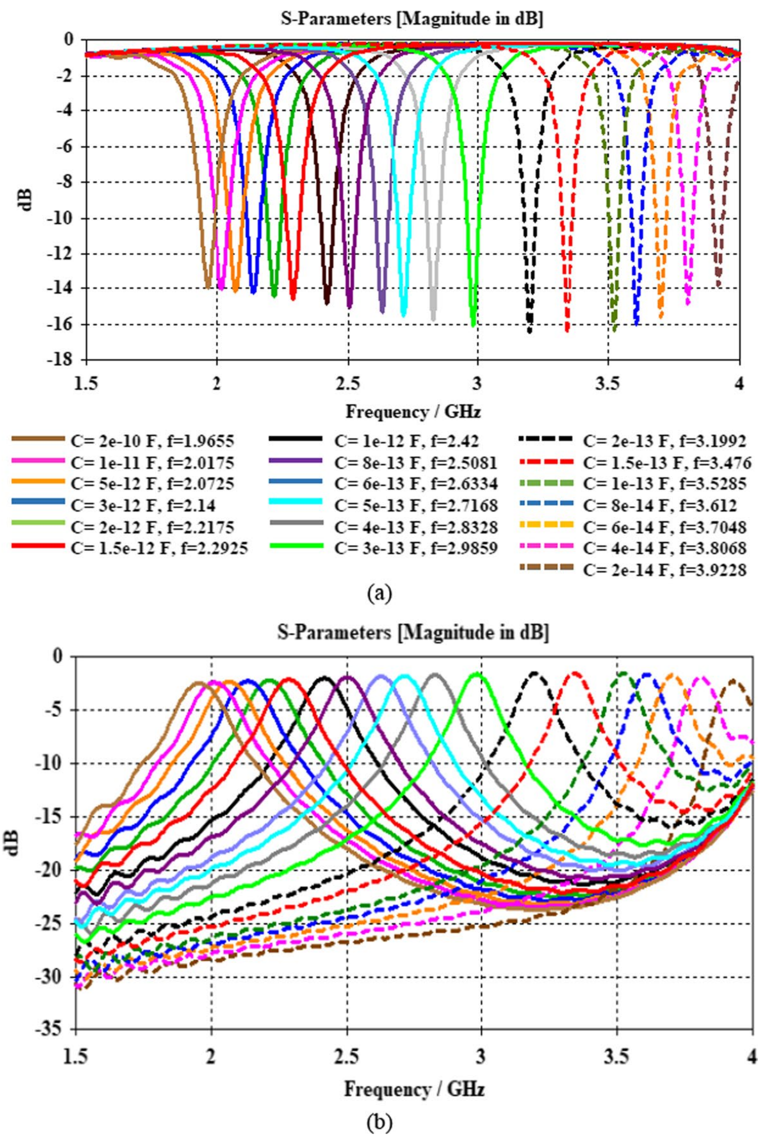

Fig. 16 The suggested tunable BPF's simulated scattering parameters, **a** Return loss $|S_{11}|$ and **b** Transmission coefficient $|S_{12}|$

Table 3 The suggested tunable BPF's 10 dB BW and IL at various resonance frequencies

Resonance frequency (GHz)	10dB BW (MHz)	IL (dB)
1.9655	59	− 2.2
2.2925	55	− 2
2.7165	50	− 1.7
2.985	48	− 1.5
3.7	40	− 1.6
3.9	35	− 2.1

Coupled varactor diode-loaded SOLR and microstrip line geometry was chosen due to the good resonant frequency reconfiguration sensitivity when the varactor diode connected across the SOLR gap has its capacitance changed due to the application of the reverse bias voltage (VR). This proposed filter construction is compatible with the design of the planar monopole antenna presented in section A and can be easily incorporated into the antenna's feed line.

2.4 Combining the tunable BPF and the WB antenna

In this subsection, the design of the suggested tunable filtenna is presented. As shown in Fig. 17c, d, the tunable BPF is inserted into the feed line of the WB antenna to create the tunable filtenna. Table 4 contains the suggested filtenna's dimensions in mm. Impedance matching among the radiating patch and the BPF is made easier by this configuration while reducing system size and expense. A comparison between the simulated $|S_{11}|$ versus frequency of the antenna and the suggested filtenna at a single tuning voltage is plotted in Fig. 18. It is noted that the combination of the BPF with the antenna enables the wide band antenna to operate at a narrowband state with high selectivity, while the simulated $|S_{11}|$ versus frequency of the tunable filtenna at various tuning voltages is shown in Fig. 19. The achieved tuning frequency band is 1.63 GHz, which spans the range from 1.93 to 3.56 GHz.

The result of the varactor reverse bias voltage (VR) on the frequency, efficiency, and 10 dB BW of the suggested filtenna is depicted in Table 5. It is evident that the filter has high selectivity with narrow bandwidths ranging from 39.9 to 53 MHz over the entire tuning voltage range from 0 Volt to 30 Volt. Figures 20 and 21 provide clarification on the impact of the BPF's insertion loss, and the losses caused by lumped elements, such as the varactor diode and choke coil, on the filtenna's efficiency and realized gain in dBi. Table 6 compares the suggested filtenna parameters to the freestanding WB antenna numerically. The realized gain and efficiency of the filtenna ranged from 0.7 to 2.26 dBi and 49 to 60%, respectively, within the tuning range.

3 Results and discussion

Figure 22 shows the manufactured prototype of the suggested tunable filtenna. Utilizing the Agilent E3620A DC power supply and the vector network analyzer (VNA) Rohde & Schwarz ZVB 20, the $|S_{11}|$ parameters have been measured. The measured and simulated $|S_{11}|$ are compared in Fig. 23, and it is seen that there are small frequency changes between them. In all instances of tuning voltages, the percentage error in resonance

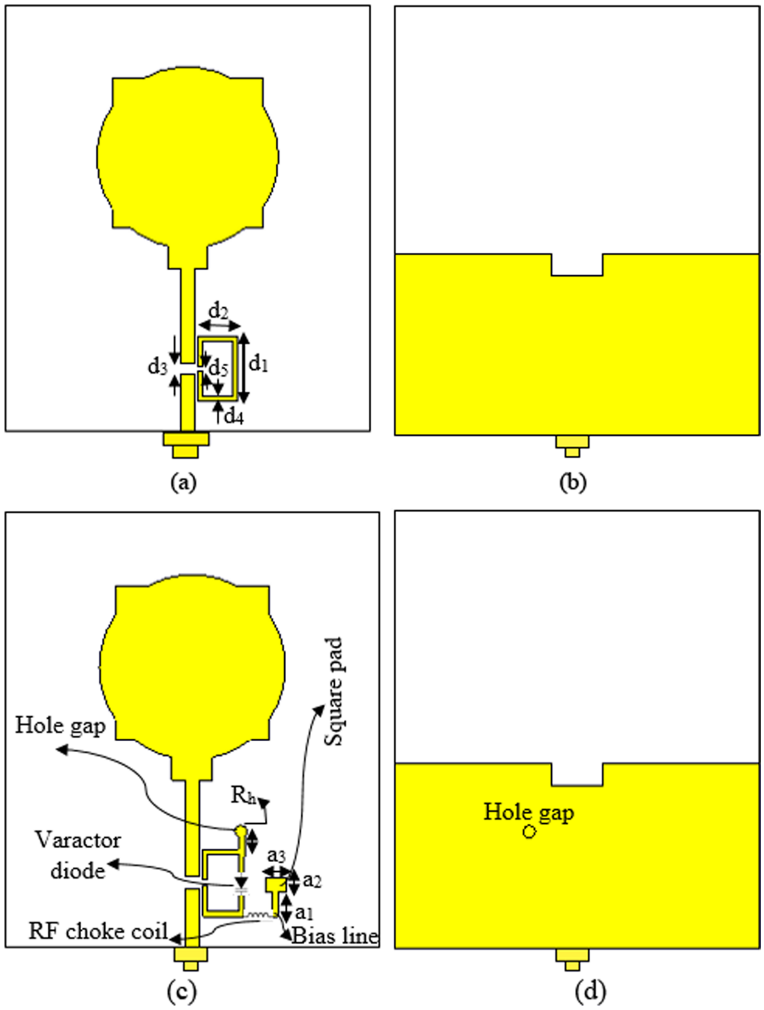

Fig. 17 Suggested filtenna construction **a** Front view of filtenna, **b** Back view of filtenna, **c** Front view of tunable filtenna, and **d** Back view of tunable filtenna

Table 4 Dimensions of the proposed filtenna in mm

Parameter	**Value** (mm)	**Parameter**	**Value** (mm)
d_1	8	a_1	4
d_2	5.5	a_2	2
d_3	1. 5	a_3	3
d_4	0.75	R_h	1
d_5	0.75		

frequency does not routinely exceed 5%, where the percentage error can be defined as $(\frac{f_{\text{measured}}-f_{\text{simulated}}}{f_{\text{measured}}}) \times \%$.

The suggested filtenna was tested to extract the radiation patterns outcomes inside the anechoic chamber as shown in Fig. 24. Figure 25 compares the suggested filtenna's simulated and measured normalized radiation patterns at $\phi = 0^{\circ}$ and $\phi = 90^{\circ}$ planes at the two different frequencies $f = 2.37$ GHz and $f = 3.03$ GHz. It should be observed that

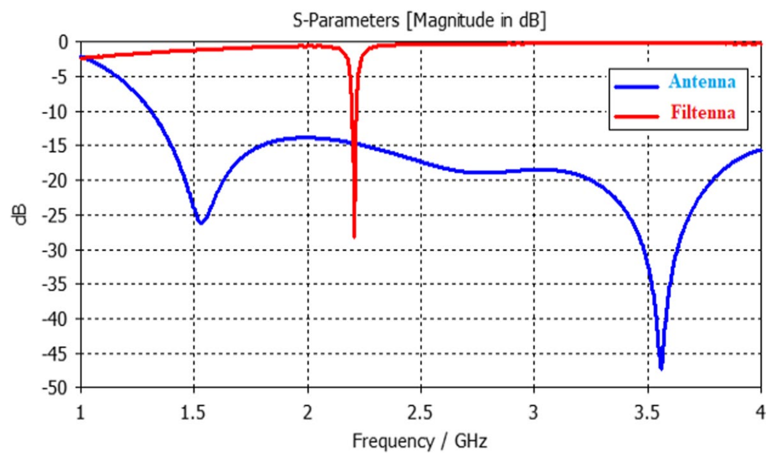

Fig. 18 Simulated |*S*11| parameter of the antenna and filtenna element at single tuning voltage

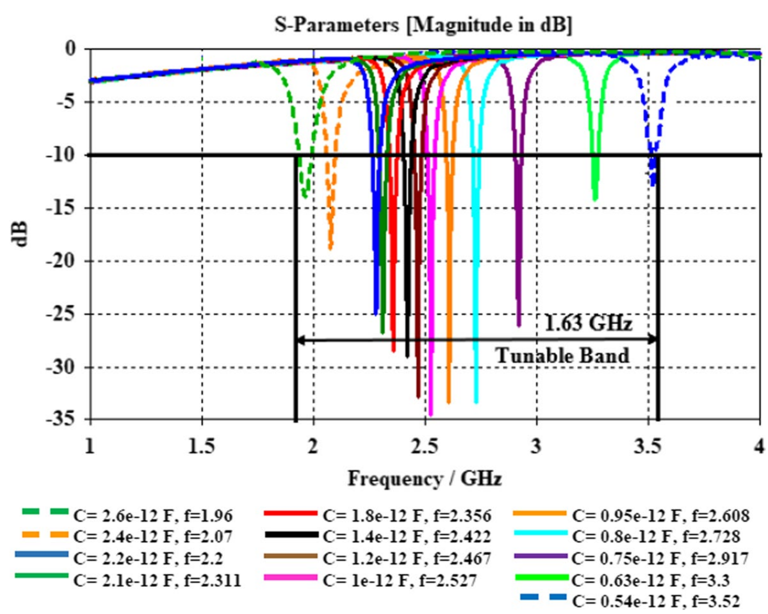

Fig. 19 Simulated |*S*11| parameter of the tunable filtenna element at various tuning voltages

Table 5 The result of the varactor reverse bias voltage (VR) on the frequency, efficiency, and 10 dB BW of the suggested filtenna

Reverse voltage VR (Volt)	Capacitance (PF)	Frequency (GHz)	Efficiency (%)	10dB BW (MHz)
0	2.6	1.96	59	53
2.5	1.4	2.422	60	34
4.5	0.95	2.608	60	33.9
10	0.75	2.917	58	40.3
20	0.63	3.3	55	33.9
30	0.54	3.52	49	45

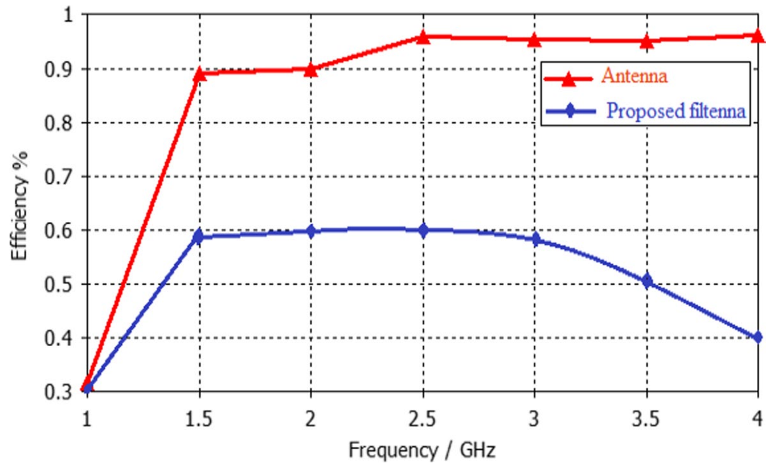

Fig. 20 The suggested filtenna's and the WB antenna's simulated efficiency

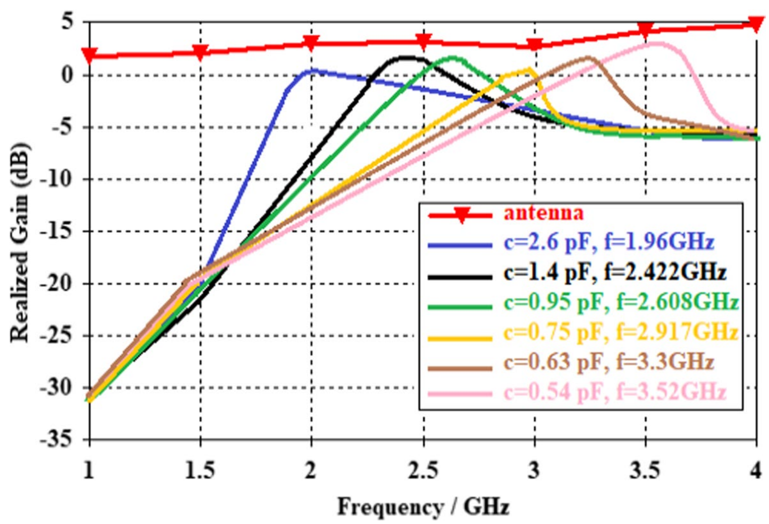

Fig. 21 The WB antenna's and the suggested filtenna's simulated realized gain

Table 6 The effectiveness of the suggested filtenna and the WB antenna

Frequency (GHz)	**Efficiency** (%)		**Realized gain** (dBi)	
	Antenna	**Filtenna**	**Antenna**	**Filtenna**
1.96	89.9	59	2.8	0.89
2.422	95	60	3.12	1.5
2.608	95.8	60	3.05	1.39
2.917	95.4	58	2.72	0.7
3.3	95.2	55	3.53	1.03
3.52	95.6	49	4.15	2.26

the radiation pattern of the filtenna is fairly constant. Additionally, Fig. 26 compares the suggested filtenna's simulated and measured realized gains. The findings of the simulation and the measurements correspond fairly well.

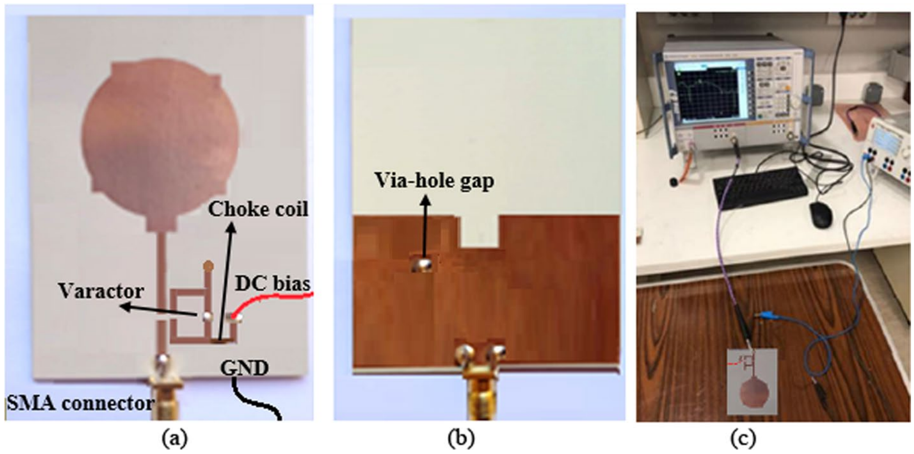

Fig. 22 Manufacture of the suggested filtenna **a** Front view, **b** Back view, and **c** Measurement setup

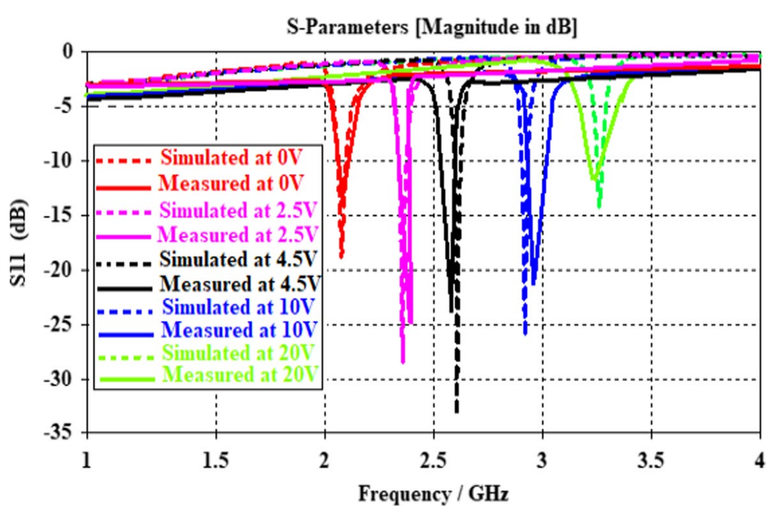

Fig. 23 The suggested filtenna's simulated and measured $|S_{11}|$ of at various tuning voltages

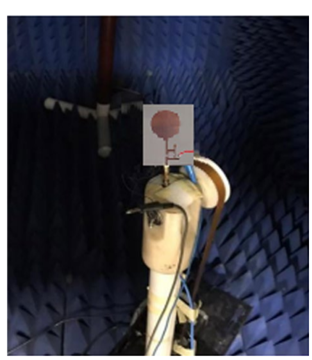

Fig. 24 The setup of the radiation patterns measurements of the filtenna

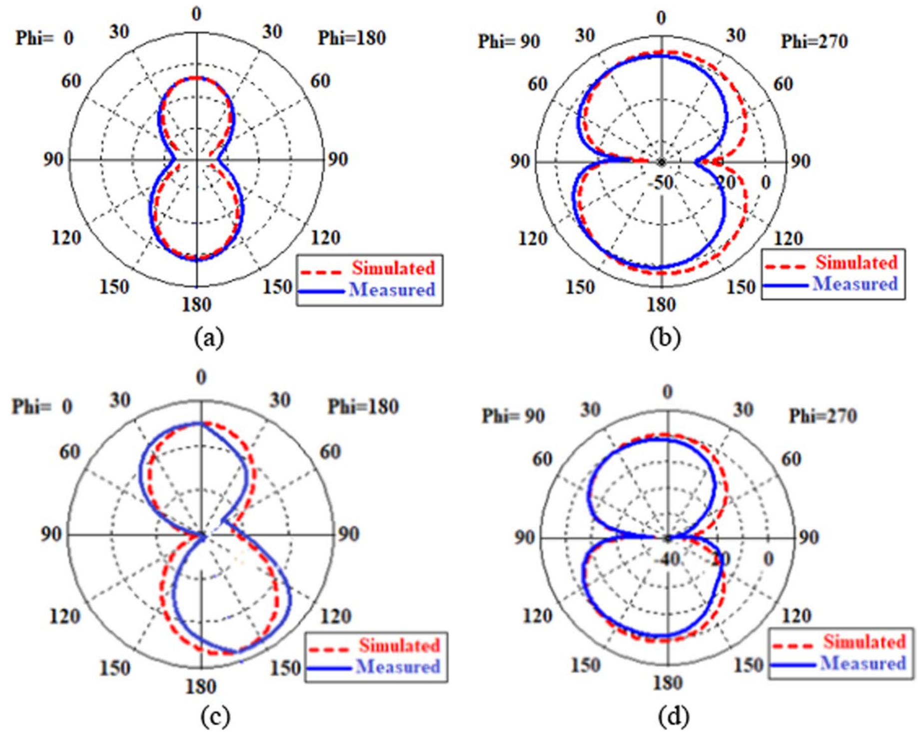

Fig. 25 The suggested filtenna's simulated and measured normalized radiation patterns at **a** $\phi = 0^{\circ}$ and **b** $\phi = 90^{\circ}$ planes at $f = 2.4GHz$ and **c** $\phi = 0^{\circ}$ and **d** $\phi = 90^{\circ}$ planes at $f = 3.3$ GHz

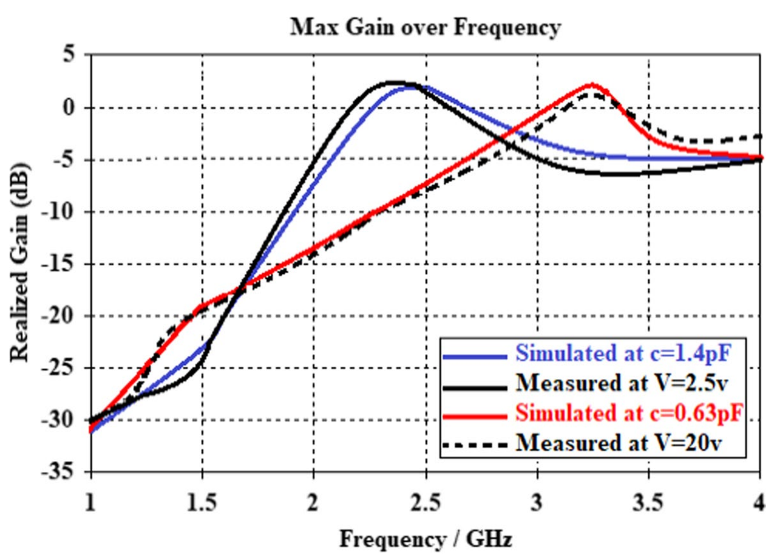

Fig. 26 The suggested filtenna's simulated and measured realized gain

4 Comparison with related works

The suggested filtenna has great performance and important characteristics in terms of size, operating frequencies (GHz), tuning band (GHz), tuning diodes numbers, efficiency, and gain compared to rows #1 up to #9 in Table 7. The comparison displays a

Table 7 Detailed comparison of latest technology of microstrip filtenna with the existing literature

#	Ref.	Size (mm^2)	Range of operating frequencies (GHz)	Tuning band (GHz)	Tuning diodes numbers	Efficiency	Gain (dBi)
1	[2]	60 × 80	1.3–3	1.7	4 varactor diode	NA	NA
2	[3]	45 × 42.5	2.37–3.69	1.33	Single varactor diode	60%	1.37
3	[15]	80 × 100	2.2–3.4	1.2	Single varactor diode	NA	NA
4	[20]	25 × 15	3.3–4.2	0.9	2 PIN diode	50%	3.5
5	[21]	39 × 42	3.63–4.7	1.07	2 PIN diode	NA	2
6	[32]	80 × 80	1.75–3	1.25	4 varactor diode	NA	4.5
7	[33]	80 × 110	1–1.6	0.6	NA	NA	2.64
8	[34]	NA	1.57–1.86	0.31	NA	NA	5
9	[35]	30 × 59.8	6.16–6.6	0.44	Single varactor diode	NA	NA
This work		25 × 35	1.93–3.56	1.63	Single varactor diode	60%	2.26

competitive version of the offered filtenna designs, which are organized in Table 7. It is evident that the suggested filtenna has a more compact construction and a wider tunable band when compared to existing filtenna.

Except for [10], the proposed filtenna has the smallest size of $(25 \times 35)\ mm^2$. On the other hand, it has the widest tuning range of width 1.63 GHz. One varactor is utilized in the design, which adds another advantage to the proposed filtenna.

5 Conclusion

This paper presented an efficient design of a wideband tunable microstrip filtenna for spectrum sensing in cognitive radio systems. The exploitation of SOLR to design a band-pass filter and its integration into a wideband antenna are discussed. The frequency tuning is accomplished electrically by joining a varactor diode into the filtenna construction. The proposed filtenna structure has a total bandwidth of 1.63 GHz and is designed for flexible frequency scanning throughout the frequency range from 1.93 to 3.56 GHz with high selectivity and narrow bandwidths ranging from 39.9 to 53 MHz. The realized gain and efficiency of the filtenna ranged from 0.7 to 2.26 dBi and 49 to 60%, respectively, within the tuning range. The simulated results agree with the measured results, demonstrating that the proposed antenna can be a good solution for spectrum sensing in CR Systems.

Abbreviations

BPF Band-pass filter
CR Cognitive radio
SS Spectrum sensing
SU Secondary user
PU Primary user
SDR Software-defined radio
UWB Ultra-wideband
CST Computer simulation technology
SOLR Square open-loop resonator

Acknowledgements

The authors would like to thank the respected editors and the reviewers for their helpful comments.

Author contributions
All authors contributed to the preparation of this manuscript. All authors conceived the original ideas presented in this work. Additionally, all authors have cooperated writing this manuscript and reviewing all parts of it. Finally, all other have been equally contributed in this work.

Funding
Open access funding provided by The Science, Technology & Innovation Funding Authority (STDF) in cooperation with The Egyptian Knowledge Bank (EKB).

Availability of data and materials
The experimental data used and/or analyzed during the current study are available from the corresponding author on reasonable request. Rania H. Elabd, Eng.rania87@yahoo.com, rania.hamdy@ndeti.edu.eg.

Declarations

Ethics approval and consent to participate
Not applicable.

Consent for publication
All authors agree to publish the research in this journal.

Competing interests
Authors declare no competing interests.

Received: 24 July 2023 Accepted: 17 October 2023
Published online: 23 October 2023

References

1. J. Liu, H. Liu, X. Dou, Y. Tang, C. Zhang, L. Wang, R. Tang, Y. Yin, A low profile, dual-band, dual-polarized patch antenna with antenna-filter functions and its application in MIMO systems. IEEE Access **9**, 101164–101171 (2021). https://doi.org/10.1109/ACCESS.2021.3096969
2. A.A. Ibrahim, H.A. Mohamed, A.R. Rizo, R.P. Michel, H. Aboushady, Tunable filtenna with DGS loaded resonators for a cognitive radio system based on an SDR transceiver. IEEE Access **10**, 32123–32131 (2022). https://doi.org/10.1109/ACCESS.2022.3160467
3. H.S. Fouda, A.H. Hussein, Practical implementation of real-time cognitive radio energy detector using frequency reconfigurable filtenna. J. Electromag. Waves Appl. **34**(2), 168–182 (2019). https://doi.org/10.1080/09205071.2019.1692699
4. R. Indrakanti, E. Elias, Low complexity spectrum sensing technique for cognitive radio using farrow structure digital filters. Eng. Sci. Technol. Int. J. **22**(1), 131–142 (2019)
5. R.H. Elabd, A.J.A. Al-Gburi, SAR assessment of miniaturized wideband MIMO antenna structure for millimeter wave 5G smartphones. Microelectron. Eng. **282**, 112098–112115 (2023). https://doi.org/10.1016/j.mee.2023.112098
6. R.H. Elabd, H.H. Abdullah, A high isolation UWB MIMO vivaldi antenna based on CSRR-NL for contemporary 5G millimeter-wave Applications. J. Infrared Milli Terahz Waves **43**, 920–941 (2022). https://doi.org/10.1007/s10762-022-00894-y
7. R.H. Elabd, H.H. Abdullah, M. Abdelazim, Compact highly directive MIMO vivaldi antenna for 5G millimeter-wave base station. J Infrared Milli Terahz Waves **42**, 173–194 (2021). https://doi.org/10.1007/s10762-020-00765-4
8. R.H. Elabd, H.H. Abdullah, M. Abdelazim, A. Abotalb, A. Shaban, Studying the performance of linear precoding algorithms based on Millimeterwave MIMO communication system. Int. J. Sci. Eng. Res. (IJSER) **10**(1), 2076–2082 (2019)
9. R.H. Elabd, H.H. Abdullah, M. Abdelazim, A. Abotalb, A. Shaban, Low complexity high- performance precoding algorithms for mm-Wave MU-MIMO communication system. Wirel. Pers. Commun. (2020). https://doi.org/10.1007/s11277-020-07692-6
10. L. Yang, H. Su, C. Zhong, Z. Meng, H. Luo, X. Li, Y. Yan Tang, Y. Lu, Hyperspectral image classification using wavelet transform-based smooth ordering. Int. J. Wavelets Multiresolut. Inf. Process. **17**(6), 1950050 (2019)
11. X. Zheng, Y. Yan Tang, J. Zhou, A framework of adaptive multiscale wavelet decomposition for signals on undirected graphs. IEEE Trans. Signal Process. **67**(7), 1696–1711 (2019)
12. X. Liu, H. Zhang, Y. Cheung, X. You, Y. Yan Tang, Efficient single image dehazing and denoising: an efficient multi-scale correlated wavelet approach. Comput. Vis. Image Understand. **162**, 23–33 (2017)
13. E. Guariglia, S. Silvestrov, Fractional-Wavelet Analysis of Positive definite Distributions and Wavelets on D′(C), in *Engineering Mathematics II*, Springer, pp. 337–353, 2016
14. E. Guariglia, Harmonic sierpinski gasket and applications. Entropy **20**(9), 714 (2018)
15. J. Araujo, M. Oliveira, C. Filho, C. Silva, M.S. Coutinho, Reconfigurable filtenna using varactor diode for wireless applications. J. Microw. Optoelectron. Electromag. Appl. **20**(4), 834–854 (2021)
16. H.A. Elhady, A. Elkorany, S.A. Saad, New simple flower shaped reconfigurable bandnotched UWB antenna using single varactor diode. Prog. Electromagn. Res. **76**, 197–206 (2017). https://doi.org/10.2528/PIERC17061507
17. M. Chun, Z. Wen, H. Wang, Compact, frequency-reconfigurable filtenna with sharply defined wideband and continuously tunable narrowband states. IEEE Trans. Antenna Propag. **65**, 5026–5034 (2017). https://doi.org/10.1109/TAP.2017.2736535

18. H. Atallah, A. Abdel-Rahman, K. Yoshitomi, Compact frequency reconfigurable filtennas using varactor loaded T-shaped and H-shaped resonators for cognitive radio applications. IET Microw. Antenna Propag. **10**, 991–1001 (2016). https://doi.org/10.1049/iet-map.2015.0700
19. M. LukGK, A band-reconfigurable antenna based on directed dipole. IEEE Trans. Antenna Propag. **64**, 64–71 (2014). https://doi.org/10.1109/TAP.2013.2287520
20. W.A. Awan, S.I. Naqvi, W.A.E. Ali, N. Hussain, A. Iqbal, H.H. Tran, M. Alibakhshikenari, E. Limiti, Design and realization of a frequency reconfigurable antenna with wide, dual, and single-band operations for compact sized wireless applications. Electronics **10**, 1321–1332 (2021). https://doi.org/10.3390/electronics10111321
21. P.P. Shome, T. Khan, Sh.K. Koul, M.M. Antar, Compact UWB-to-C band reconfigurable filtenna based on elliptical monopole antenna integrated with bandpass filter for cognitive radio systems. IET Microw. Antennas Propag. **14**(10), 1079–1088 (2020). https://doi.org/10.1049/iet-map.2019.0819
22. M.A. Abdelghany, W.A.E. Ali, H.A. Mohamed, A.A. Ibrahim, Filtenna with frequency reconfigurable operation for cognitive radio and wireless applications. Micromachines (2023). https://doi.org/10.3390/mi14010160
23. J. Choi, S. Park, J. Lee, K.Y. Jung, UHF-printed monopole filtenna for partial discharge detection with LTE signal suppression. J. Electromag. Eng. Sci. **23**(2), 180–187 (2023). https://doi.org/10.26866/jees.2023.2.r.158
24. H. Tang, J.X. Chen, H. Chu, Integration design of filtering antenna with load-insensitive multilayer balun filter. IEEE Trans. Compon. Packag. Manuf. Technol. **9**(6), 1408–1416 (2016)
25. Y. Tawk, J. Costantine, C. Christodoulou, A varactor-based reconfigurable filtenna. IEEE Antenna Wirel. Propag. Lett. **11**, 716–719 (2012)
26. Y. Qin, F. Wei, Y. Guo, A wideband-to-narrowband tunable antenna using a reconfigurable filter. IEEE Trans. Antenna Propag. **63**, 2282–2285 (2015)
27. K.R. Mahmoud, A.M. Montaser, Design of compact mm-wave tunable filtenna using capacitor loaded trapezoid slots in ground plane for 5G router applications. IEEE Access **8**, 27715–27723 (2020). https://doi.org/10.1109/ACCESS.2020.297160
28. J. Yun, S.T. Van, J.Y. Park, Y. Yang, K.Y. Lee, K.C.H. Hwang, Cavity-backed patch filtenna for harmonic suppression. IEEE Access **8**, 221580–221589 (2020). https://doi.org/10.1109/ACCESS.2020.3043320
29. S. Kingsly, D. Thangarasu, M. Kanagasabai, M.G.N. Alsath, S.K. Palaniswamy, T.R. Rao, S. Subbaraj, Y.P. Selvam, P. Sambandam, G. Ganesan, Tunable band-notched high selective UWB filtering monopole antenna. IEEE Trans. Antennas Propag. **67**(8), 5658–5661 (2019). https://doi.org/10.1109/TAP.2019.2920997
30. F. Wei, X.B. Zhao, X.W. Shi, A balanced filtering quasi-yagi antenna with low cross-polarization levels and high common-mode suppression. IEEE Access **7**, 100113–100119 (2019). https://doi.org/10.1109/ACCESS.2019.2931141
31. W. Ahmad, D. Budimir, UWB filtennas with dual bandnotch for WiMAX and WLAN bands using circular and square resonators. IET Microw. Antenna Propag. (2016). https://doi.org/10.1049/ic.2016.0004
32. T.L. Wu, Y.M. Pan, P.F. Hu, S.Y. Zheng, Design of a low profile and compact omnidirectional filtering patch antenna. IEEE Access **5**, 1083–1089 (2017). https://doi.org/10.1109/ACCESS.2017.2651143
33. T.L. Wu, Y.M. Pan, P.F. Hu, Wideband omnidirectional slotted patch antenna with filtering response. IEEE Access **5**, 26015–26021 (2017). https://doi.org/10.1109/ACCESS.2017.2768067
34. A. Ramadan, K. Kabalan, J. Costantine, A tunable filtenna for cognitive radio applications, in *9th European conference on antennas and propagation (EuCAP). IEEE*, pp. 1–2 2015
35. H. Nachouane, A. Najid, F. Riouch, Electronically reconfigurable filtenna for cognitive radios. Microw. Opt. Technol. Lett. **59**, 399–404 (2017)
36. A.H. Hussein, H.S. Fouda, H.H. Abdullah, A.A. Khalaf, A highly efficient spectrum sensing approach based on antenna arrayes beamforming. IEEE Access **8**, 25184–25197 (2020)
37. H.S. Fouda, M.E. Nasr, A.H. Hussein, A highly efficient approach for performance enhancement of multiple antenna elements based spectrum sensing techniques using side lobe level reduction. Alexandria Eng. **61**(8), 5983–5999 (2022)
38. M.E. Yassin, H. Mohamed, E.A. Abdallah, H.S. El-Hennawy, Semi-circular stubs UWB monopole antenna with tunable dual band-notch characteristics. Int. J. Microwave Opt. Technol. **15**(2), 169–177 (2022)
39. J. Hong, *Microstrip filters for RF/microwave applications*, 2nd edn. (Wiley, Hoboken, 2011)
40. A. Munir, B. D. Wulandari, W. Aditomo, Y. Prasetio, DGS-based UWB microstrip bandpass filter and itsequivalent circuit, in *2017 IEEE 13th Malaysia International Conference on Communications (MICC)*, pp. 70–73, 2017
41. Z. Xu, Q. Zhang, L. Guo, A compact 5G decoupling MIMO antenna based on split-ring resonators. Hindawi Int. J. Antennas Propagat. (2019). https://doi.org/10.1155/2019/3782528
42. A.A. Chinig, L. Errkik, A. El Abdellaoui, A. Tajmouati, Design of a microstrip diplexer and triplexer using open loop resonators. J. Microwaves Optoelectron. Electromag. Appl. (2016). https://doi.org/10.1590/2179-10742016v15i2602

Publisher's Note